Journal of Statistical Physics, Vol. 121, Nos. 1/2, October 2005 (© 2005)
DOI: 10.1007/s10955-005-8414-y

Voronoi Fluid Particle Model for Euler Equations

Mar Serrano,[1] Pep Español[1] and Ignacio Zúñiga[1]

Received October 12, 2004; accepted July 27, 2005

We present a fluid particle model based on the Voronoi tessellation that allows one to represent an inviscid fluid in a Lagrangian description. The discrete model has all the required symmetries and structure of the continuum equations and can be understood as a linearly consistent discretization of Euler's equations. Although the model is purely inviscid, we observe that the probability distribution of the accelerations of the Voronoi fluid particles shows the presence of tails at large accelerations, what is compatible with experimental Lagrangian turbulence observations.

KEY WORDS: Fluid particle models; Euler equations; Lagrangian turbulence.

1. INTRODUCTION

The understanding of fluid turbulence is still incomplete despite many decades of continued effort.(1) The large number of degrees of freedom involved in the phenomenon makes the attack of the problem very difficult, both theoretically and computationally. The classical scaling theory of Kolmogorov(1) predicts universality in the so called inertial range. However, deviations from the scaling predictions are observed in real fluids which are associated to the phenomenon of intermittency. A particularly interesting development towards the understanding of intermittency has come from the turbulent transport of passive scalars.(2) By following the Lagrangian trajectory of fluid particles, it has been possible to identify statistical integrals of motion that are at the root of intermittency.(2) The development of fast tracking systems has allowed to study experimentally the statistical properties of suspended particles in a turbulent flow.(3) It

[1]Depto. Física Fundamental, Universidad Nacional de Educación a Distancia, Avda. Senda del Rey 9, 28040 Madrid, Spain; e-mails: {mserrano,pep,izuniga}@fisfun.uned.es

turns out that a Lagrangian description of fluid flow is a natural one in order to get some insight on the physics of turbulence.

The aim of this paper is to study an extremely simple and appealing fluid particle model which is based on the Voronoi tessellation of space. Just by requiring that the fluid particles move according to their velocity and that the energy of the system is conserved leads naturally to the equations of motion for the reversible part of the dynamics. We show that for smooth flows, the equations are a discrete version of Euler's equations for an inviscid compressible fluid. We observe that the model presents statistical features that are very similar to experimental measurements of fluid tracers in fully developed homogeneous turbulence. Of course, our model is purely reversible, with no dissipation and, therefore, cannot be considered as a proper model for turbulence, not even in the limit of infinite Reynolds number. As it is well known, the limit of infinite Reynolds number is singular and, therefore, no matter how small are the dissipative terms in the Navier–Stokes equations, they play a crucial role, either in boundary layers or in setting a viscous length scale in homogeneous turbulence, the Kolmogorov scale. Nevertheless, in this paper we explore to what extent, the inviscid equations already capture statistical features of real turbulence.

2. EULER EQUATIONS FOR AN INVISCID FLUID

Euler's equations describe the dynamics of a compressible inviscid fluid and have the following form

$$\partial_t \rho = -\nabla\cdot\rho\mathbf{v}, \qquad \partial_t \rho\mathbf{v} = -\nabla\cdot\rho\mathbf{v}\mathbf{v} - \nabla P, \qquad \partial_t s = -\nabla\cdot s\mathbf{v}, \tag{1}$$

where $\rho = \rho(\mathbf{r}, t)$ is the mass density field, $\mathbf{v} = \mathbf{v}(\mathbf{r}, t)$ the velocity field, $s = s(\mathbf{r}, t)$ the entropy density field and $P = P^{\text{eq}}(\rho(\mathbf{r}, t), s(\mathbf{r}, t))$ the pressure field which, according to the local equilibrium assumption, is given by the equilibrium equation of state evaluated at the non-equilibrium values of the mass and entropy density fields. The Euler's equations can be expressed in the Lagrangian point of view by introducing Lagrangian coordinate $\mathbf{R}(\mathbf{r}, t)$ as the solution of the equation

$$\partial_t \mathbf{R}(\mathbf{r}, t) = \mathbf{v}(\mathbf{R}(\mathbf{r}, t), t), \tag{2}$$

with initial condition $\mathbf{R}(\mathbf{r}, 0) = \mathbf{r}$. We introduce the volume field as the solution of the following equation

$$\frac{d}{dt}\mathcal{V}(\mathbf{R}(\mathbf{r}, t), t) = \mathcal{V}(\mathbf{R}(\mathbf{r}, t), t)\nabla\cdot\mathbf{v}(\mathbf{R}(\mathbf{r}, t), t), \tag{3}$$

which is the equation for the rate of change of an infinitesimal volume that is transported by a flow field $\mathbf{v}(\mathbf{r}, t)$. We introduce the *extensive* mass $M(\mathbf{r}, t)$, momentum $\mathbf{P}(\mathbf{r}, t)$ and entropy $S(\mathbf{r}, t)$ fields which are related to the density fields by $\rho(\mathbf{r}, t) = M(\mathbf{r}, t)/\mathcal{V}(\mathbf{r}, t)$, $\rho\mathbf{v}(\mathbf{r}, t) = \mathbf{P}(\mathbf{r}, t)/\mathcal{V}(\mathbf{r}, t)$, $s(\mathbf{r}, t) = S(\mathbf{r}, t)/\mathcal{V}(\mathbf{r}, t)$. In terms of these extensive fields Eqs. (1) become simply

$$\frac{d}{dt}M = 0, \qquad \frac{d}{dt}\mathbf{P} = -\mathcal{V}\nabla P, \qquad \frac{d}{dt}S = 0. \tag{4}$$

These equations are remarkably simple and physically they express the fact that the environment seen as we follow the flow is one in which the mass and the entropy remain constant and the forces on that environment are just pressure forces. Some textbooks[4] prefer to start from the physics expressed in Eqs. (4) in order to deduce Eqs. (1).

3. THE FLUID PARTICLE MODEL

Our aim now is to formulate a discrete model of the Euler equations that is as close to Eqs. (4) in structure as possible. To this end we introduce N fluid particles that represent the whole fluid system. The state of these particles is characterized by their positions $\mathbf{R}_i$, momenta $\mathbf{P}_i$, entropy S_i and mass M_i. Each fluid particle has also some derived quantities like the volume $\mathcal{V}_i$, the velocity $\mathbf{V}_i = \mathbf{P}_i/M_i$ and the internal energy $\mathcal{E}_i$. The volume $\mathcal{V}_i$ of the fluid particle is a geometric quantity given as a function of the positions of the particles $\mathcal{V}_i(\mathbf{R}_1, \ldots, \mathbf{R}_N)$, whereas the internal energy is, through the local equilibrium hypothesis, a function of the extensive variables of the fluid particle (mass, entropy and volume), this is $\mathcal{E}_i = \mathcal{E}(M_i, S_i, \mathcal{V}_i)$. In this sense, a fluid particle is considered as a small thermodynamic subsystem characterized by the equation of state. This equation of state governs the thermodynamic behavior of the fluid particles, and so, associated to each fluid particle we can also define a temperature T_i and a pressure P_i. The total energy of the system is defined as

$$E = \sum_i \left[\frac{\mathbf{P}_i^2}{2M_i} + \mathcal{E}(M_i, S_i, \mathcal{V}_i) \right]. \tag{5}$$

Now we turn to the dynamics of the state variables. We postulate the following equations of motion

$$\dot{\mathbf{R}}_i = \mathbf{V}_i, \qquad \dot{M}_i = 0, \qquad \dot{S}_i = 0. \tag{6}$$

The first equation mimics the Lagrangian equation (2), whereas the last two equations represent the corresponding continuum equations (4). The momentum equation follows from the requirement that the energy[5] is conserved, i.e. $\dot{E}=0$. This leads to

$$M_i \dot{\mathbf{V}}_i = \sum_j \frac{\partial \mathcal{V}_j}{\partial \mathbf{R}_i} P_j. \tag{7}$$

We still have to specify the volume of a fluid particle as a function of the positions of the fluid particles. Before making a selection we note that any sensible selection for the volume of the fluid particles must be translationally and rotationally invariant, this is

$$\begin{aligned} \mathcal{V}_i(\mathbf{R}_1, \ldots, \mathbf{R}_N) &= \mathcal{V}_i(\mathbf{R}_1 + \mathbf{a}, \ldots, \mathbf{R}_N + \mathbf{a}), \\ \mathcal{V}_i(\mathbf{R}_1, \ldots, \mathbf{R}_N) &= \mathcal{V}_i(\boldsymbol{\Lambda}\mathbf{R}_1, \ldots, \boldsymbol{\Lambda}\mathbf{R}_N), \end{aligned} \tag{8}$$

where $\mathbf{a}$ is an arbitrary vector and $\boldsymbol{\Lambda}$ is an arbitrary rotation matrix. If we take the derivative of the first equation in (8) with respect to $\mathbf{a}$ and evaluate the result at $\mathbf{a}=0$ and of the second equation with respect to $\boldsymbol{\Lambda}$ and evaluate it at $\boldsymbol{\Lambda}=\mathbf{1}$, we have the identities

$$\sum_i \frac{\partial \mathcal{V}_j}{\partial \mathbf{R}_i} = 0, \qquad \sum_i \mathbf{R}_i \times \frac{\partial \mathcal{V}_j}{\partial \mathbf{R}_i} = 0. \tag{9}$$

These equations imply that Eqs. (6) and (7) conserve total linear momentum $\mathbf{P}=\sum_i \mathbf{P}_i$ and total angular momentum defined as $\mathbf{L}=\sum_i \mathbf{R}_i \times \mathbf{P}_i$. Note, however, that the invariance under rotation is broken if the container has no rotational symmetry, as it happens in systems with periodic boundary conditions. Total mass and total entropy are trivially conserved by Eqs. (6) and (7). The invariance of the energy under permutation of the particle labels leads to a quasi-conservation law of a discrete form of the circulation, as has been shown in refs. 5 and 6.

As a final remark, we note that Euler's equations (1) have a Hamiltonian structure[7–9] and it can be shown that the discrete model described by Eqs. (6) and (7) has also a Hamiltonian structure.[10] Note that

$$-\frac{\partial \mathcal{E}}{\partial \mathbf{R}_i} = \sum_j \frac{\partial \mathcal{V}_j}{\partial \mathbf{R}_i} P_j, \tag{10}$$

where $\mathcal{E}$ is the internal energy of the whole system. Therefore, Eqs. (6) and (7) have the form of a molecular dynamics where the internal energy $\mathcal{E}$ plays the role of an "effective potential energy" that depends on the positions in a many-body form through the volumes of the fluid particles. The conservation of linear and angular momentum follows from the invariance of the energy with respect to translations and rotations. Note that the energy (Eq. (5)) depends on the position of the fluid particles only through the volumes of the fluid particles.

All the above properties make the proposed model very appealing from a theoretical point of view but, of course, the discrete model has been proposed just *by analogy* with the continuum model. However, we show below that the particle algorithm is a discretization of the Euler equations to second-order in the spatial discretization length, this is,

$$-\frac{1}{\mathcal{V}_i}\sum_j \frac{\partial \mathcal{V}_j}{\partial \mathbf{R}_i} P_j \approx (\nabla P)(\mathbf{R}_i). \tag{11}$$

Before proceeding to prove Eq. (11) we still have to specify the actual dependence of the volume of each fluid particle on the positions of the neighboring fluid particles. A first possibility leads to the smoothed particle hydrodynamics or dissipative particle dynamics approach, where the volume is given by the inverse of the density $\mathcal{V}_i = d_i^{-1}$.[11] The density d_i of the fluid particle, in turn, is defined in terms of a weight function $W(r)$ of finite support, this is, $d_i = \sum_j W(r_{ij})$, where r_{ij} is the distance between particles i, j. The volume thus defined satisfies Eq. (8). The problem with this approach is that Eq. (11) is only satisfied if the range of the weight function is *very* large. Typically a fluid particle needs to interact with ~ 70 neighbors in 2D and ~ 150 in 3D, which amounts to a large computation time.

A second possibility is the definition of the volume of the fluid particles through the Voronoi tessellation. In this case, the volume of a given fluid particle corresponds to the volume of the region that is closer to that fluid particle than to any other particle in the system. In this way, a partition of space in non-overlapping cells that cover all the space is achieved. The tessellation also provides a concept of local neighborhood and, typically, a fluid particle has six neighbors in 2D and 12 in 3D. In addition, a quite remarkable property of the Voronoi tessellation is that for *linear fields* of the form $P(\mathbf{r}) = a + \mathbf{b}\cdot\mathbf{r}$, where a is a constant scalar and $\mathbf{b}$ is a constant vector, Eq. (11) is not approximate but *exact*. Note that the gradient of the linear pressure field is given by the vector $\mathbf{b}$. Then we claim that

$$-\frac{1}{\mathcal{V}_i}\sum_j \frac{\partial \mathcal{V}_j}{\partial \mathbf{R}_i}\left[a+\mathbf{b}\cdot\mathbf{R}_j\right]=\mathbf{b}. \tag{12}$$

In order to proof this *linear consistency property*, (Eq. (12)), we need several results concerning the Voronoi tessellation. The first one is the derivative of the volume with respect to the position of the cells, which takes the values (see ref. 12)

$$\frac{\partial \mathcal{V}_j}{\partial \mathbf{R}_i}=-A_{ij}\left(\frac{\mathbf{c}_{ij}}{R_{ij}}-\frac{\mathbf{e}_{ij}}{2}\right) \quad \text{for } i\neq j, \quad \frac{\partial \mathcal{V}_i}{\partial \mathbf{R}_i}=\sum_{j\neq i} A_{ij}\left(\frac{\mathbf{c}_{ij}}{R_{ij}}-\frac{\mathbf{e}_{ij}}{2}\right). \tag{13}$$

Here, A_{ij} is the area of the face of contact between cells i and j, $\mathbf{c}_{ij}$ is the position of the center of mass of the face of contact between cells i and j with respect to the point $(\mathbf{R}_i+\mathbf{R}_j)/2$ and $\mathbf{e}_{ij}$ is the unit vector pointing from particle j to particle i. Note that the vector $\mathbf{c}_{ij}$ is parallel to the face i, j, whereas $\mathbf{e}_{ij}$ is perpendicular to it. The following highly non-trivial results are also relevant. For every cell i not at the boundary of the system, we have

$$\sum_j A_{ij}\mathbf{e}_{ij}=0, \qquad -\frac{1}{\mathcal{V}_i}\sum_j A_{ij}\mathbf{C}_{ij}^{\mu}\mathbf{e}_{ij}^{\nu}=\delta^{\mu\nu}, \tag{14}$$

where $\mathbf{C}_{ij}=\mathbf{c}_{ij}+(\mathbf{R}_i+\mathbf{R}_j)/2$ is the position of the center of mass of the face joining cells i, j. The proofs of the identities (14) are presented in the Appendix A. By using Eqs. (13) and (14) on the left-hand side of (11) we easily arrive at the conclusion that (11) is true for arbitrary meshes (that is, for any fluid particle configuration). The remarkable property in Eq. (12) shows that we have a discrete representation of the gradient operator that produces exact results for linear fields. This shows that the identity in Eq. (11) is valid to second-order in the spatial discretization length. The linear consistency property is one of the main results of this paper, as it shows that the discrete model formulated on physical grounds can be interpreted as a Lagrangian discretization of the continuum Euler equations (1) which is second-order in space. Other Voronoi discretizations (ref. 13) do not share this very appealing property and lead, actually, to unphysical numerically unstable simulations in the limit of zero viscosity.

4. SIMULATION RESULTS

We have numerically solved Eqs. (6) and (7) in two dimensions. These equations are closed with the equation of state for an ideal gas and we

will use the units described in ref. 12. In order to check whether the particle model does actually simulates an inviscid fluid, we have conducted a simulation in which initially the particles are in a triangular lattice and the initial velocity profile is a transverse sinusoidal wave. For a viscous fluid, this type of perturbation decays in an exponential way with a time scale that is inversely proportional to the viscosity. For an inviscid fluid the perturbation would never decay. However, this type of perturbation is unstable due to the existence of an inflection point in the flow. What we observe in our simulations, as shown in left Fig. 1 is that the perturbation does not decay for quite a long time. To be more specific, the sinusoidal perturbation decays with a viscosity which within the errors of the simulation is of the order of 10^{-10}, i.e., virtually zero in the units selected as in ref. 12. After some time, the particles at the inflection point start to acquire off-planar components and the system eventually gets completely disordered with a chaotic movement of the particles as the final behavior. This behavior is characteristic of all the simulations we have conducted and is a reflection that almost any Euler flow is completely unstable.[14] It is certainly very difficult to show that a particular numerical method for solving Euler's equations produces correct results, due to the intrinsic unstable character of these equations which reflects in the development of singularities in finite time, not cured by the presence of a dissipative mechanism. We have conducted simulations of the decay of an initial transverse sinusoidal velocity profile by introducing viscous forces as described in ref. 12, and have measured the viscosity from the decay time. In this case, the simulations are stable. By plotting the measured viscosity versus the input viscosity we may infer the value of the effective viscosity in the limit of

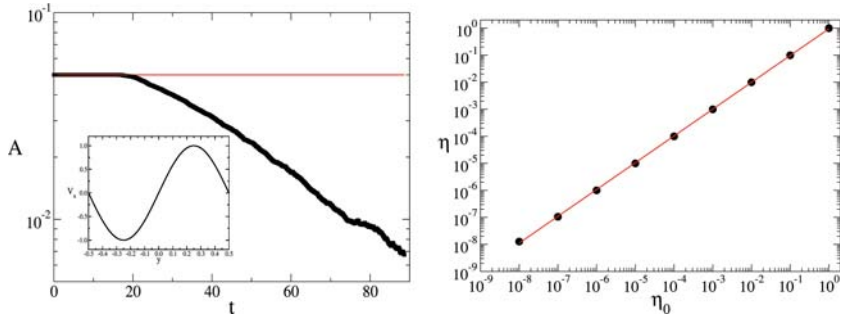

Fig. 1. Left: Amplitude of an initial transverse sinusoidal velocity field as a function of time. The amplitude remains constant until the flow becomes unstable around time 20, near the inflection point. Right: Viscosity η measured from the decay in time of a transverse sinusoidal velocity versus input viscosity η_0 when the model includes viscous forces. The extrapolation of the straight line of unit slope shows that the inviscid particle model does actually model an inviscid fluid.

zero input viscosity. The result is plotted in right Fig. 1 and it shows that for this smooth flow we have a well defined limit of zero input viscosity leading to zero measured viscosity.

The system described by Eqs. (6) and (7) reaches a dynamical equilibrium state apparently similar to the usual one in Molecular Dynamics simulations. One would be tempted to describe this non-dissipative final state as a *compressible homogeneous turbulence* state corresponding to an infinite Reynolds number (formal limit of zero viscosity). That this is not entirely the case can be quantified by measuring the kinetic energy spectrum. While in the Kolmogorov theory it is given by a power law, in our case it is a flat spectrum corresponding to spatial white noise.

A quantity of recent interest in the field of turbulence is the distribution of accelerations of fluid tracers due to the presence of unusual tails in the distribution showing that it is very probable to have high-values for the acceleration.[3,15] We have compiled from our simulation results the distribution of accelerations in the dynamical equilibrium state of our Voronoi fluid particles in a box with periodic boundary conditions. A typical example of the acceleration distribution in logarithmic scale as a function of the acceleration divided by the square root of its variance is presented in left Fig. 2. Note that the distribution has tails at high-accelerations that extend much further than they would for a Gaussian distribution with the same variance. The flatness factor $\langle a^4\rangle/\langle a^2\rangle$ of this distribution takes a value around 7.75, suggesting that the acceleration of the fluid particles

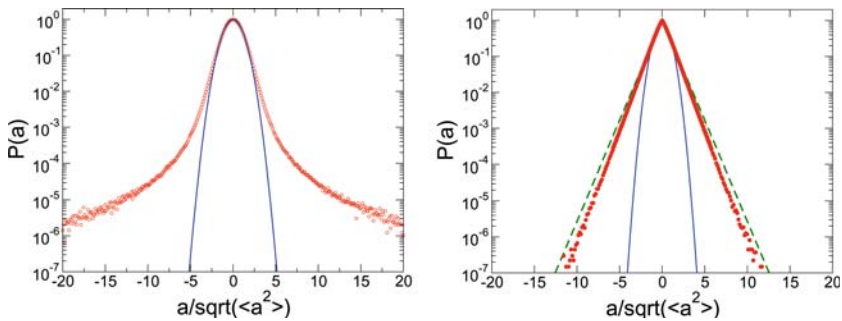

Fig. 2. Left: In circles the Voronoi acceleration distribution in the so called dynamical equilibrium state. The probability density function is normalized by its standard deviation. A best Gaussian fit at the region of large probability is also shown. Big accelerations appear in the system quite often, as compared to those in a Gaussian distribution. This distribution corresponds to a simulation of $N=2500$ fluid particles with a total energy of $E=1.0025$ in reduced units. Right: Acceleration distribution $P(a)$ in logarithmic scale as a function of $a/\langle a^2\rangle^{1/2}$ for a Lennard–Jones system. Circles correspond to simulation results, continuum line is the best Gaussian fit and the dashed line corresponds to an exponential fit.

is an intermittent variable (for Gaussian distributions the flatness factor is 3). The authors in ref. 3 make the observation that in fully developed turbulence the viscous damping term in Navier–Stokes equations is small compared to the pressure gradient term and, therefore, the acceleration is closely related to the pressure gradient. This may be the reason why our discrete model still captures this intriguing feature of developed turbulence.

In order to see the relevance of the numerical result for the accelerations in the Voronoi discrete model, we compute the acceleration distributions in a Molecular Dynamics simulation for a purely repulsive Lennard–Jones type interaction (the WCA potential, see ref. 16). The thermodynamic state of the system corresponds to a typical liquid condition given by $\rho = 0.844$ for the fluid density and $T = 0.71$ for the temperature (in conventional reduced units in MD for Argon) while the number of molecules is $N_T = 1000$. The results for the probability distribution for the accelerations $P(a)$ as a function of the accelerations divided by the square root of its variance is shown in right Fig. 2. This distribution function has an exponential form. The Molecular Dynamics distribution is very different from the one for the Voronoi fluid particle model.

In order to get a better insight into the dynamics of this discrete fluid particle model, we have also computed the velocity autocorrelation function of the fluid particles. To analyze the results, we introduce two velocity scales in our reduced units, the speed of sound for an ideal gas $c = \sqrt{2T}$, where T is the mean temperature of the system, and the kinetic velocity $\overline{v}_k = \sqrt{2K}$, where K is the mean total kinetic energy of the system. From these two velocities, we can extract two time scales related to the time it takes a particle to travel with a particular velocity its typical particle linear size l_0. The linear size l_0 of a particle is equal to the typical interparticle distance. It can be measured from the first peak of the radial distribution function plotted in Fig. 3. The two timescales are a sonic time $\tau_c = l_0/c$ and a kinetic time $\tau_k = l_0/\overline{v}_k$.

The typical velocity autocorrelation function $C(t) = \langle \mathbf{v}(t) \cdot \mathbf{v}(0) \rangle$ is plotted in Fig. 4. The autocorrelations are normalized with the initial value, this is, $C(t)/C(0)$. The oscillation at short times in the velocity autocorrelation function occurs at the sonic time scale and it is a reflection of the compressibility of the model. The ulterior evolution corresponds to an exponential decay with a time scale corresponding to the kinetic time scale. To show this, we have conducted three simulations at the same thermodynamic state with different number of particles (Fig. 5). We see that the smaller particle size forgets quicker its initial velocity value. We have also conducted simulations with the same number of particles and different kinetic average energy. The corresponding velocity

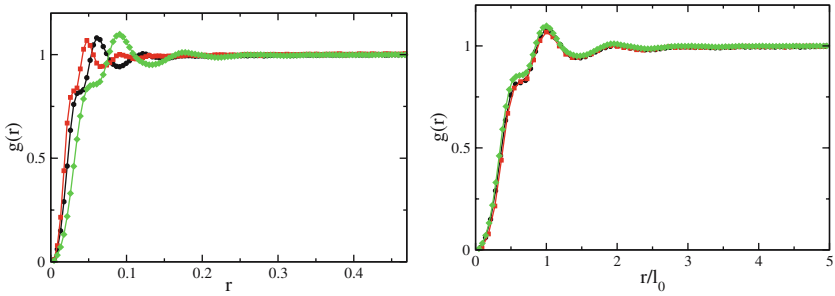

Fig. 3. Pair correlation function $g(r)$ for the same thermodynamic state, for increasing number of fluid particles $N = 400, 900, 1600$ (left). The curves collapse into a master curve if we rescale the distance with l_0 (right).

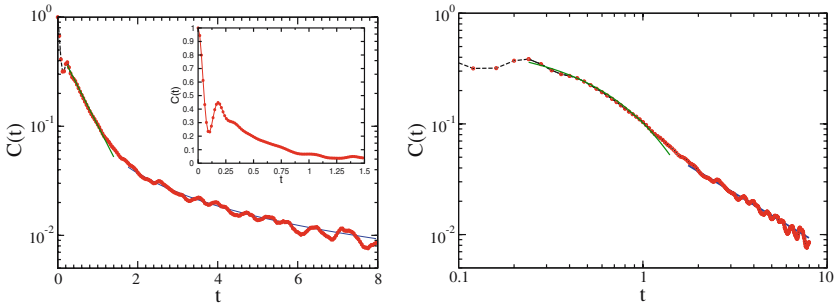

Fig. 4. Left: Log–lin plot of the typical behavior of the velocity autocorrelation function in time. Detail at short times is shown in the inset picture. Right: Log–log representation of the left figure in which two regimes after the sonic scale are clearly distinguished, first an exponential decay and for longer times an algebraic dependence (the solid lines are the corresponding fits). This second regime has to do with the celebrated hydrodynamic long time tail t^{-1}.

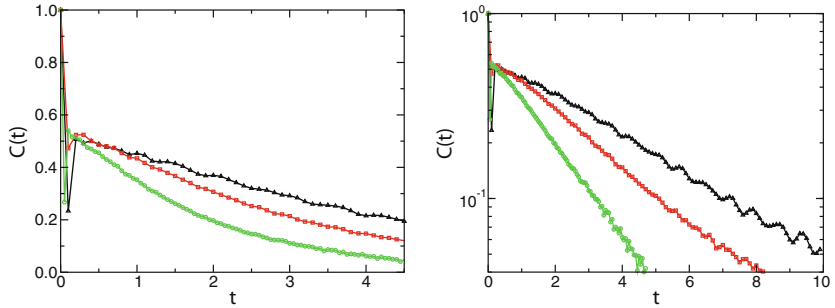

Fig. 5. Left: Normalized velocity autocorrelation function for a fixed total energy and three different resolutions $N = 400, 900, 1600$ in the same box. Right: Log-lin plot of the left figure, where the exponential decay is apparent.

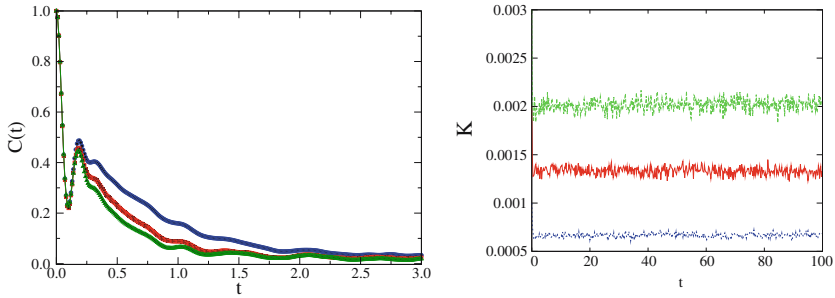

Fig. 6. Left: Velocity autocorrelation function for three different total kinetic energies and the same number of fluid particles $N = 400$. Top line corresponds to the smaller mean total kinetic energy. Right: Kinetic energies as a function of time. A fixed internal energy $\mathcal{E}_0 = 1$ has been chosen for the three simulations and the selected initial values are $K_0 = 1, 2, 3 \times 10^{-3}$, respectively.

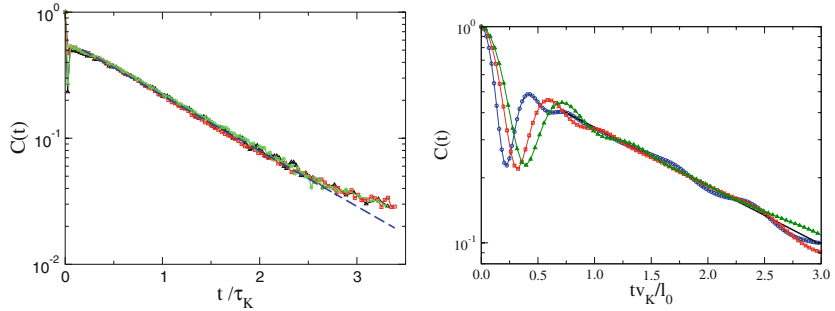

Fig. 7. Velocity correlation functions rescaled by the $C(t)/\overline{v}_k^2$ as a function of the rescaled time t/τ_k. Left picture corresponds to Fig. 5 and right picture to Fig. 6. After the sonic time, they all lie on a master curve that can be fitted to an exponential.

autocorrelation functions are plotted in Fig. 6. All the autocorrelation functions can be collapsed into a single one in the region of exponential decay when we rescale $C(t)/\overline{v}_k^2$, and t/τ_k. This is shown in Fig. 7.

5. CONCLUSIONS

We have presented a Lagrangian fluid particle model for the simulation of Euler's equations based on a Voronoi tessellation. The model is very elegant and simple, and we show that it is a faithful representation of Euler's equation *whenever the velocity field is smooth*. Of course, a purely inviscid fluid readily develops instabilities.[14] Onsager conjectured that the fully developed velocity field of the Euler's equation can even be

non-differentiable.[17,18] In the fluid particle model this non-differentiability can be assimilated to the chaotic and random motion of the final dynamic equilibrium state of the fluid particles. For a chaotic distribution of velocities, one would conclude that it is not possible to define a derivative of the velocity field. Even though the model is purely reversible, the system has, *at a coarse-grained level*, an associated viscosity, in the same way as a Lennard–Jones system (governed by Newtons' reversible equations of motion) has a viscosity (which is a parameter that appears in the hydrodynamic equations). A given system may be described by reversible or irreversible dynamic equations depending on the detail of the level of description.

The conclusion of the simulations is that the only relevant length in the system is fixed by the fluid particle size (l_0), and the exponential decay of the velocity autocorrelation function only depends on this scale and the kinetic velocity.

Despite of the fact that our model cannot be taken as the inviscid limit of the viscous Navier–Stokes equations, which is singular, we observe in the model several statistical features that actually correspond to similar features observed in experiments on Lagrangian tracers in homogeneous fully developed turbulence. In particular, we have observed that the fluid particle velocity autocorrelation function shows an exponential decay beyond the sonic scale. The characteristic decay time scales with the kinetic time scale. The higher the kinetic energy of the fluid particles (which is a measure of the intensity of this "turbulence"), the fastest is the decay. As mentioned in ref. 19, the exponential decay dictates a Lagrangian time scale that appears as a time characteristic of the energy injection. This seems to be also our case, where the kinetic time scale τ_k plays the role of the experimental Lagrangian time scale, related to the intensity of this "turbulence". The acceleration distribution function reveals large tails that extend much further than they would for a Gaussian distribution with the same variance. All these results agree with recent experimental results.[3,15] One possible explanation for this agreement is that in fully developed turbulence, the viscous damping term in Navier–Stokes equations is small compared to the pressure gradient term and therefore, the acceleration is closely related to the pressure gradient, which is the only force in our model.

APPENDIX A. MATHEMATICAL PROPERTIES OF THE VORONOI TESSELLATION

In this appendix, we summarize some mathematical properties of the Voronoi tessellation. Other interesting results and more detailed definitions concerning the Voronoi tessellation can be found in the appendix of ref. 12. The Voronoi tessellation is a geometrical construction associated to

a collection of N points in space, named cell centers or nodes, which have positions $\{\mathbf{R}_1, \ldots, \mathbf{R}_N\}$. The tessellation associates to every point the region of space that it is closer to that point than to any other point of the collection. This produces a partition of the space into a cellular structure. The common wall between two neighbor cells are, by definition, at equal distance of the nodes of each cell and it is perpendicular to the vector $\mathbf{R}_{ij} = \mathbf{R}_i - \mathbf{R}_j$ joining the nodes.

In this note, we will make extensive use of the smooth characteristic function $\chi_i(\mathbf{r})$ re-introduced by Flekkøy and Coveney,[20] and which are known in a different context as Shephard functions. The smoothed characteristic function of the Voronoi cell i is defined as

$$\chi_i(\mathbf{r}) = \frac{\Delta(|\mathbf{r} - \mathbf{R}_i|)}{\sum_j \Delta(|\mathbf{r} - \mathbf{R}_j|)}, \tag{A.1}$$

where the function $\Delta(r) = \exp\{-r^2/2\sigma^2\}$ is a Gaussian of width σ. This characteristic function satisfies the relations

$$\frac{\partial \chi_i(\mathbf{r})}{\partial \mathbf{r}} = \frac{1}{\sigma^2} \sum_j \chi_i(\mathbf{r}) \chi_j(\mathbf{r}) (\mathbf{R}_i - \mathbf{R}_j), \qquad \sum_j \frac{\partial \chi_i}{\partial \mathbf{R}_j} = -\frac{\partial \chi_i}{\partial \mathbf{r}}. \tag{A.2}$$

We can introduce the space average of a function $f(\mathbf{r})$ over the Voronoi cell i

$$[f]_i = \frac{1}{\mathcal{V}_i} \int d\mathbf{r} \chi_i(\mathbf{r}) f(\mathbf{r}) \quad \mathcal{V}_i = \int d\mathbf{r} \chi_i(\mathbf{r}), \tag{A.3}$$

where $\mathcal{V}_i$ is the volume of the ith Voronoi cell.
Consider now the cell average of the divergence of an arbitrary vector field $\mathbf{A}(\mathbf{r})$, this is

$$\begin{aligned} [\nabla \cdot \mathbf{A}]_i &= \frac{1}{\mathcal{V}_i} \int d\mathbf{r} \chi_i(\mathbf{r}) \nabla \cdot \mathbf{A}(\mathbf{r}) \\ &= \frac{1}{\mathcal{V}_i} \int_{\partial V} d\mathbf{S} \cdot \mathbf{A}(\mathbf{r}) \chi_i(\mathbf{r}) - \frac{1}{\mathcal{V}_i} \int d\mathbf{r} \mathbf{A}(\mathbf{r}) \cdot \nabla \chi_i(\mathbf{r}), \end{aligned} \tag{A.4}$$

where we have made use of Gauss' theorem. The first surface integral over the boundary of the full domain will vanish if the cell i does not cross this boundary (in which case the characteristic function of cell i vanishes for all points of the boundary).

By using the first relation in Eq. (A.2) we have

$$[\nabla\cdot\mathbf{A}]_i = -\frac{1}{\mathcal{V}_i}\int d\mathbf{r}\mathbf{A}(\mathbf{r})\cdot\nabla\chi_i(\mathbf{r})$$
$$= \frac{1}{\mathcal{V}_i}\sum_j \mathbf{R}_{ij}\frac{1}{\sigma^2}\int d\mathbf{r}\mathbf{A}(\mathbf{r})\chi_i(\mathbf{r})\chi_j(\mathbf{r}). \tag{A.5}$$

First, let us assume that the vector field is just constant. Its divergence will be simply zero. This implies the following identity

$$0 = -\frac{1}{\mathcal{V}_i}\sum_j \mathbf{R}_{ij}\frac{A_{ij}}{R_{ij}}\cdot\mathbf{A}, \tag{A.6}$$

where we have introduced

$$A_{ij} = R_{ij}\frac{1}{\sigma^2}\int d\mathbf{r}\chi_i(\mathbf{r})\chi_j(\mathbf{r}). \tag{A.7}$$

This quantity A_{ij} becomes in the limit $\sigma\to 0$ the area of the face of contact between cells i, j. Equation (A.6) becomes then $\sum_j A_{ij}\mathbf{e}_{ij} = 0$, where $\mathbf{e}_{ij}$ is the unit vector normal to the face i, j. Therefore, $A_{ij}\mathbf{e}_{ij}$ is the "surface vector" of face i, j. In words, $\sum_j A_{ij}\mathbf{e}_{ij} = 0$ states that for any given Voronoi cell not on the boundary of the system, the sum of the "surface vectors" over the cell vanish.

Second, let us assume that the vector field $\mathbf{A}(\mathbf{r})$ depends linearly on the positions, this is, $\mathbf{A}(\mathbf{r}) = \mathbf{\Lambda}\cdot\mathbf{r}$, where $\mathbf{\Lambda}$ is a constant matrix. Substitution in Eq. (A.5) leads to

$$\mathrm{tr}\mathbf{\Lambda} = -\frac{1}{\mathcal{V}_i}\sum_j \mathbf{R}_{ij}\cdot\mathbf{\Lambda}\cdot\frac{1}{\sigma^2}\int d\mathbf{r}\chi_i(\mathbf{r})\chi_j(\mathbf{r})\mathbf{r}$$
$$= -\frac{1}{\mathcal{V}_i}\sum_j A_{ij}\mathbf{e}_{ij}\mathbf{C}_{ij}:\mathbf{\Lambda}, \tag{A.8}$$

where the double dot means double contraction. The vector $\mathbf{C}_{ij}$ is defined through this very equation and is, in the limit $\sigma\to 0$ the position of the center of mass of the face i, j. For arbitrary matrices $\mathbf{\Lambda}$ (and, in particular, for those matrices $\mathbf{\Lambda}$ with only one single entry different from zero), Eq. (A.8) holds if and only if

$$-\frac{1}{\mathcal{V}_i}\sum_j A_{ij}\mathbf{e}_{ij}\mathbf{C}_{ij} = \mathbf{1}, \tag{A.9}$$

where $\mathbf{1}$ is the identity matrix.

ACKNOWLEDGMENTS

This work has been supported by the Spanish Ministerio de Educación y Ciencia with the Grant No FIS2004-01934. We thank Mariano Revenga for his visualization program PUNTO.

REFERENCES

1. U. Frisch, *Turbulence* (Cambridge University Press, 1995).
2. G. Falkovich, K. Gawedzki, and M. Vergassola, Particles and fields in fluid turbulence, *Rev. Mod. Phys.* **73**:913 (2001).
3. A. L. Porta, G. A. Voth, A. M. Crawford, J. Alexander, and E. Bodenshatz, Fluid particle accelerations in fully developed turbulence, *Nature* **409**:1017 (2001).
4. L. D. Landau and E. M. Lifshitz, *Fluid Mechanics* (Pergamon Press, 1959).
5. J. J. Monaghan, Sph compressible turbulence, *Mon. Not. R. Astron. Soc.* **335**(3):843–852 (2002).
6. J. J. Monaghan and D. Price, Variational principles for relativistic smoothed particle hydrodynamics, *Mon. Not. R. Astron. Soc.* **328**(3):381–392 (2001).
7. H. Lamb, *Hydrodynamics*, 6th ed. (Cambridge University Press, 1932).
8. G. A. Kuz'min, Ideal incompressible hydrodynamics in terms of the vortex momentum density, *Phys. Let.* **96A**:88–90 (1983).
9. V. I. Osledets, On a new way of writing the Navier Stokes equation: The Hamiltonian formalism, *Russ. Math. Surveys* **44**:210–211 (1989).
10. P. Español, M. Serrano, and H. C. Öttinger, Thermodynamically admissible form for discrete hydrodynamics, *Phys. Rev. Lett.* **83**:4542 (1999).
11. P. Español and M. Revenga, Smoothed dissipative particle dynamics, *Phys. Rev. E* **67**:026705 (2003).
12. M. Serrano and P. Español, Thermodynamically consistent mesoscopic fluid particle model, *Phys. Rev. E* **64**:046115 (2001).
13. I. Wenneker, A. Segal, and P. Wesseling, Computation of compressible flows on unstructured staggered grids, (2000) in *ECCOMAS 2000 (Barcelona)*, E. Onate, G. Bugeda and B. Suarez.
14. S. Friedlander and A. Lipton-Lifschitz, Localized instabilities in fluids, *Handbook of Mathematical Fluid Dynamics, 2003 – math.uic.edu*.
15. N. Mordant, J. Delour, E. Léveque, A. Arnéodo, and J. F. Pinton, Long time correlations in Lagrangian dynamics: A key to intermittency in turbulence, *Phys. Rev. Lett.* **89**:254501–1 (2002).
16. J. D. Weeks, D. Chandler, and H. C. Andersen, The Role of Repulsive Forces in Determining the Equilibrium of Simple Liquids, *J. Chem. Phys.* **54**:5237 (1971).
17. L. Onsager, Statistical hydrodynamics, *Nuovo Cimento*, **VI**:280–287 (1949).
18. G. L. Eyink, Energy dissipation without viscosity in ideal hydromechanics, i. Fourier analysis and local energy transfer, *Physica D* **78**:222–240 (1994).
19. N. Mordant, P. Metz, O. Michel, and J.-F. Pinton, Measurement of Lagrangian velocity in fully developed turbulence, *Phys. Rev. Lett.* **87**:214501–1 (2001).
20. E. G. Flekkøy and P. V. Coveney, From molecular to dissipative particle dynamics, *Phys. Rev. Lett.* **83**:1775 (1999).